RESEARCH

Sc$_2$O$_3$ on sapphire all-crystalline grating–waveguide resonant reflectors

Georgia Mourkioti[1] · Danish Bashir[3] · Goby A. Govindassamy[1] · Fangfang Li[2] · Robert W. Eason[1] · Thomas Graf[3] · Marwan Abdou Ahmed[3] · Jacob I. Mackenzie[1]

Abstract

This paper reports the fabrication and first demonstration of all-dielectric crystalline grating–waveguide reflectors comprising a Sc$_2$O$_3$ waveguide grown on a sub-wavelength-patterned sapphire substrate. Rigorous coupled-wave analysis is employed to simulate the operation of the structure, suggesting a 100% resonance reflectivity in theory. Structuring of the sapphire substrate is achieved using inductively coupled plasma etching, whilst pulsed laser deposition is used for epitaxial growth of the Sc$_2$O$_3$ crystalline waveguide. Devices with distinct TE- and TM-polarisation resonances around 1030-nm for an angle of incidence near 10° are demonstrated, with reflectance approaching 90%. The discrepancy in reflectivity is attributed to the waveguide thickness variation and surface roughness. Refinement of the fabrication processes and tolerances should lead to improvement in the surface quality of the crystalline grating–waveguide structure and operation closer to the ideal resonance reflectivity.

1 Introduction

The demand for reliable polarised narrow-bandwidth high-power lasers has motivated the development of innovative diffractive optics that can meet such parameters. Resonant grating–waveguide structures (GWS) [1] are the combination of a planar waveguide and a sub-wavelength grating that can be used as a polarisation-selective, highly dispersive, and high-efficiency reflector. Our motivation is to capitalise on the characteristics of GWS but using all-dielectric materials that are suitable for high-power laser cavity components,

Georgia Mourkioti and Danish Bashir have contributed equally to this work.

✉ Georgia Mourkioti
  G.Mourkioti@soton.ac.uk

  Marwan Abdou Ahmed
  abdou.ahmed@ifsw.uni-stuttgart.de

  Jacob I. Mackenzie
  jim@soton.ac.uk

1   Optoelectronics Research Centre, University
    of Southampton, Southampton SO17 1BJ, UK

2   University of Eastern Finland, 80100 Joensuu, Finland

3   Institut für Strahlwerkzeuge, University of Stuttgart,
    70569 Stuttgart, Germany

as demonstrated in [2]. GWS have been utilised for intra-cavity wavelength selection and spectral stabilisation using resonant diffraction [3] and resonant reflection [3, 4]. However, one challenge faced for resonant reflectors is that their maximum operating power (fluence) is limited by the intrinsic absorption, damage threshold of the deposited waveguide materials, as well as the low thermal conductivity of the substrate. Specifically, in several previous works, the materials used for the fabrication of such devices were mainly a combination of SiO$_2$ and Ta$_2$O$_5$ on a fused silica substrate where the GWS was able to tolerate a power density of up to 125 kW/cm^2 in resonant diffraction mode [3], 15 kW/cm^2 for the single-layer resonant reflector [4] and 52 kW/cm^2 for the multi-layer resonant reflector [5].

In this work, we report on the first resonant reflectors based on GWS made entirely of all-dielectric crystalline materials, specifically, scandium oxide (Sc$_2$O$_3$) epitaxially grown on a structured sapphire (α-Al$_2$O$_3$) substrate. These devices are similar to those of Si-on-quartz (SOQ) systems that capitalise on the all-crystalline nature of the component materials [6]. However, the intrinsic absorption in semiconductor materials at the wavelengths of interest for high-power lasers would limit their utility. Instead, all-dielectric crystalline materials as employed here have an order-of-magnitude higher thermal conductivity than silica, the typical mirror substrate used [2–5]. Potentially, these

devices offer better thermal resilience in high-power operation assuming that the intrinsic absorption is comparable with standard dielectric GWS. Moreover, we have demonstrated that the crystalline Sc_2O_3 films have a high laser damage threshold [7]. The expectation is that all-dielectric crystalline GWS devices could enable operation at powers much higher than conventional materials currently allow. In this study a GWS design, targeting laser operation at 1030 nm that is compatible with Yb:YAG thin-disc lasers was investigated.

2 Methodology

The methodology to develop the all-dielectric all-crystalline grating–waveguide resonant reflector (CGWRR) follows a three-part approach: the design, fabrication, and characterisation. The design phase was based upon previous works [2] employing rigorous coupled-wave analysis of the structure [8, 9]. In fabrication, as the grating structures must be sub-wavelength, nanofabrication processes needed to be developed and implemented. A shallower grating depth is required if only the substrate is etched, rather than the top surface of the Sc_2O_3 layer; therefore, only structuring of the sapphire substrate was investigated. Subsequently, optimisation of the conformal Sc_2O_3 waveguide growth on the structured surface via pulsed laser deposition (PLD) needed to be undertaken. Finally, characterisation comprised monitoring the surface topography during the various fabrication steps, along with determining the efficiency of the CGWRR with respect to its design specifications.

2.1 Design

Key to the operation of the CGWRR is the mechanism of coupling incident light from free space to a waveguide mode via the GWS and its subsequent outcoupling that constructively interferes with the Fresnel reflection. Only for a specific combination of wavelength, polarisation, and angle of incidence (AOI) of the incident laser beam, will the excited waveguide mode have a resonance with the grating structure to enable outcoupling into free space and lead to perfect reflection. In its simplest geometry, the GWS can be composed of a single waveguide layer surrounded by a lower index cover (typically air) and substrate layers. However, the resonance can also be achieved in diffraction or transmission by proper design of the structure [10].

The device reported here comprises a sub-wavelength grating etched into a sapphire substrate on which an epitaxially grown thin-film waveguide layer of Sc_2O_3 is deposited (Fig. 1). As illustrated in Fig. 1, a guided mode can be excited by a laser beam incident upon a grating on the surface of the planar optical waveguide, for which there is a
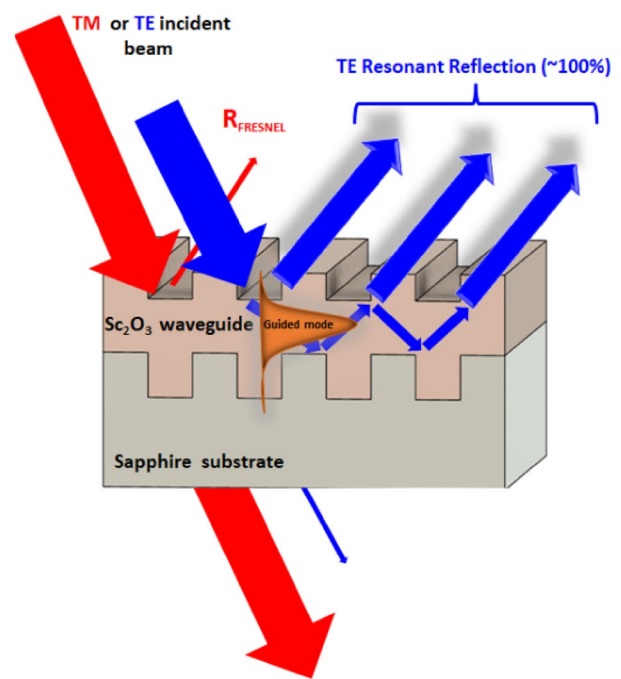

Fig. 1 Schematic and operation of CGWRR structure for a TE resonance

resonant reflection when its propagation constant is in phase with the grating such that the out-coupled light interferes constructively. To reach the ideal reflectivity, the waveguide must have no loss and the grating strength and periodicity should be constant. Consequently, very tight tolerances must be met in terms of the structuring and the quality of the waveguide material to achieve a highly efficient resonant reflection [4, 11, 12].

Rigorous coupled-wave analysis [2, 8, 9] was used to determine the CGWRR opto-geometrical parameters for operation at 1030 nm. The simulation was conducted in the same manner as described in [8, 13–16]. The main steps followed in the simulation process were: (1) design a single-layer or multi-layer waveguide that provides the desired background response (reflectivity/transmission at the laser wavelength) and (2) incorporate a grating, first choosing the duty cycle (DC) to realise effective material properties then setting the grating period to place the resonance at the desired wavelength.

In practice, the CGWRR comprises a 10×10 mm^2 c-cut sapphire ($n_o = 1.755$ and $n_e = 1.747$ [17]) substrate with a thickness of 650 µm. The nominal design parameters of the grating are an etch-depth, d, of 100 nm, a grating period $\Lambda = 515$ nm, and a duty cycle (DC) of 50%, being the ridge width, w, over the period (Λ), DC = w/Λ. On top of the structured sapphire, a 400-nm-thick Sc_2O_3 ($n = 1.972$ [18]) film was grown via PLD. The CGWRR is designed to be highly reflective at an angle of incidence of $\theta_{inc} = 10.2^o$ for

TE polarised light at a wavelength of 1030 nm. Based on the design, the calculated reflectance at 1030 nm for the two polarisations are $R_{TE} > 99.9\%$ and $R_{TM} < 10\%$ (Fresnel reflection). The spectral width of the reflection peak is around 2-nm FWHM. Figure 2a shows the design parameters for the CGWRR, whilst Fig. 2b provides the calculated spectral response of the device for light incident at an angle of $\theta_{inc} = 10.2°$.

2.2 Fabrication

The fabrication of a CGWRR has two parts, first, the etching of the grating structure into the surface of a sapphire substrate, followed by deposition of the crystalline waveguide on top.

2.2.1 Structuring of sapphire

Based on the target specifications as discussed in the previous section, it was necessary to develop fabrication processes that would enable the structuring of sapphire with sub-micron feature dimensions and aspect ratios (width to depth) approaching 2:1. In our experiments, 4-in. (0001) sapphire wafers were used as the substrate. In Fig. 3, we present the schematic of the developed fabrication process flow.

For the CGWRR designed for 1030-nm operation, we started with depositing a 200-nm-thick SiO_2 layer on the sapphire wafer using an RF-magnetron sputtering system (AJA International Orion). This film acts as a hard mask in the dry etching process of the substrate. An extra 50-nm-thick Cr layer was then deposited with a DC-magnetron
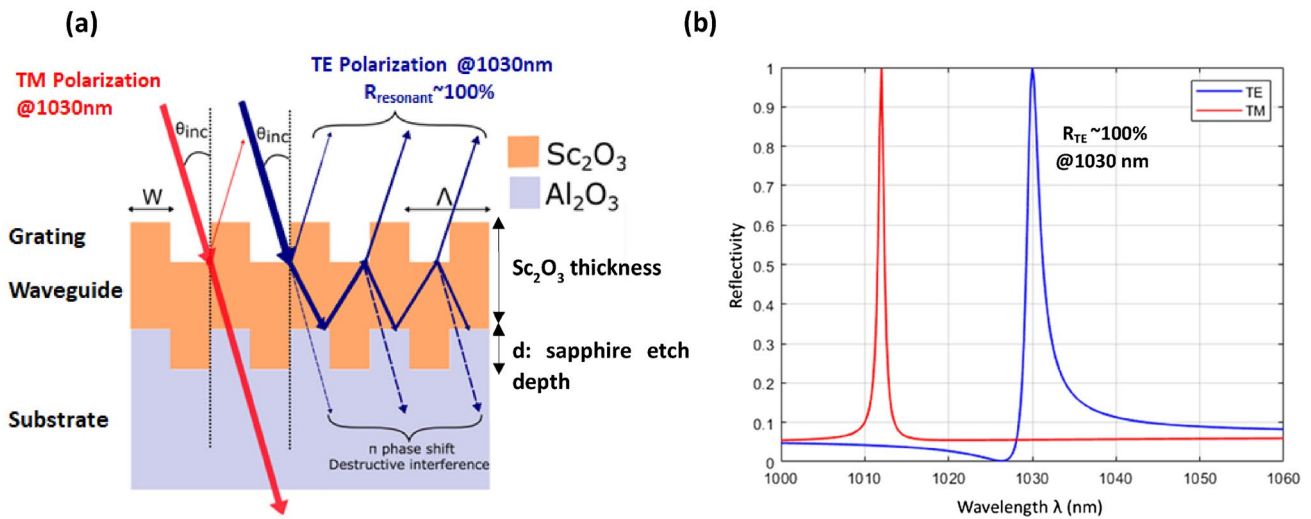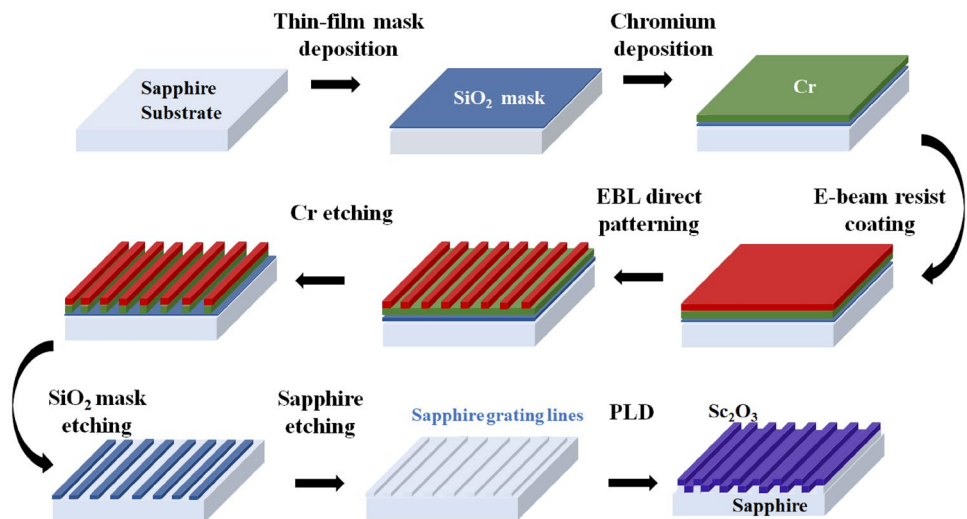
Fig. 2 **a** CGWRR design, and **b** simulation of reflectivity values in TE and TM mode

Fig. 3 Fabrication process flow diagram

sputtering system (Quorum Q300T T Plus) on top of the SiO_2, which acts as a conductive layer in the patterning process, but also as a hard mask for the dry etching of SiO_2. E-beam lithography (EBL) (Raith EBPG 5000 + ES) was used to pattern the linear gratings. Inductively Coupled-Plasma (ICP) etching with Cl_2/O_2 gas chemistry was used to etch the Cr layer, followed by O_2 plasma cleaning to remove any residual resist. ICP etching with CHF_3/Ar was then used to etch the SiO_2 layer followed by Cl_2/O_2 dry etching to remove the residual Cr layer.

At this stage, the sapphire substrate was patterned with the 200-nm-thick SiO_2 mask. Sapphire structuring was achieved using ICP etching (OPT Sys100 ICP380-Plasmalab) with $SiCl_4/Cl_2$/Ar gas chemistry, followed by immersion in hydrofluoric acid (7:1, NH_4F:HF) to remove the residual SiO_2. Dicing out a ~ 100-mm^2 chip from the wafer, the final step in the waveguide reflector fabrication process is the growth of Sc_2O_3 on top of the sapphire grating using PLD.

2.2.2 Pulsed laser deposition of Sc_2O_3

PLD is a method of choice for the rapid synthesis of sesquioxide films, as it enables the epitaxial growth of crystalline layers at a temperature around half of the melting point of their bulk-material counterparts. Figure 4a shows a schematic of the PLD chamber including the main components of the setup, whilst in Fig. 4b, we present a top view photograph of the PLD chamber during deposition. The structured sapphire chips were positioned in front of the target at a distance of (55 ± 1) mm. A CO_2 laser, operating at a wavelength of 10.6 μm, was used to heat the substrate from the rear side. The Gaussian intensity distribution of the CO_2 laser beam had been transformed by a ZnSe tetraprism into a quasi-top-hat square profile of full width equal to that of the substrate, which ensured minimal temperature

gradients are present across it [19]. For target ablation, we used a KrF excimer laser (Coherent COMPexPro 110) operating at 248 nm, with a pulse duration of ~ 25 ns and 100 Hz repetition rate. A bi-directional target ablation protocol was employed to minimise particulates, which are generated by coarsening of the target surface due to degradation by the ablation process [20]. The pulsed UV laser beam subtended an angle of incidence of 45° to the target and was focussed to a rectangular spot with an area of (6.3 ± 0.2) mm^2 at the target surface. The same target was used for all depositions to avoid any systematic differences in the deposited films.

A systematic procedure was followed for all the growths, starting with evacuation of the chamber to a pressure of 10^{-3} mbar, before introducing oxygen to reach a pressure of 2×10^{-2} mbar. The temperature of the substrate was then progressively increased to ~ 1100 °C by increasing the incident CO_2 laser power at a rate of 1 W/min. Pre-ablation of the Sc_2O_3 target was performed to remove any surface contamination before each deposition, this involved an 18,000-pulse run with equivalent parameters used for deposition whilst shielding the substrate. After each growth run, the CO_2 laser power was gradually ramped down at a rate of 0.5 W/min, which minimised the risk of the sample cracking due to thermal stress.

2.3 Characterisation

Critical to the operation of the CGWRR are the physical and optical properties of the structured substrate and waveguide layer. For this reason, the topography of these respective sections (structured sapphire and Sc_2O_3 waveguide layer) needed to be assessed during the development of the fabrication processes. Once a complete sample was produced, it was then necessary to measure its optical performance as
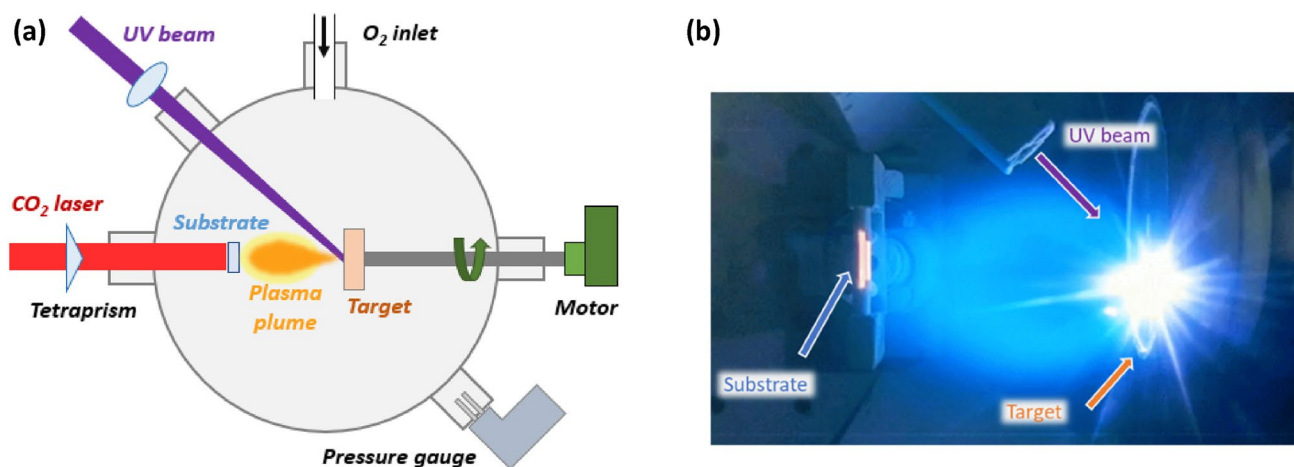

Fig. 4 **a** Top view schematic of PLD setup, and **b** top view of PLD chamber during deposition process

a reflector. Therefore, two forms of characterisation were employed during this study.

2.3.1 Surface topography investigations

The surface topography of the samples at the various process steps was measured using Atomic Force Microscopy (AFM – Park Systems AFM) or Scanning Electron Microscopy (SEM- Zeiss NVision 40). The etching of sapphire was optimised using different combinations of etching parameters during the ICP etching process, such as flow rates of the gases, RF power, ICP power and chamber pressure, all of which are specific to the individual tool. We monitored the etching profile primarily using SEM to determine the optimal etching values that could provide high etching rate, good selectivity with respect to the mask material and near-vertical profile angles.

2.3.2 Crystalline grating–waveguide resonant reflector performance

For the spectroscopic characterisation of the fabricated structures, a reflectivity measurement setup (Fig. 5) was used, employing a tuneable laser diode (1000–1070-nm wavelength range) as a source for our experiments [21]. The output of the tuneable laser was coupled to a polarisation-maintaining single-mode optical fibre, ensuring diffraction-limited beam characteristics. After collimation of the light exiting the fibre, the combination of a half-waveplate and polarising beam splitter provided control of the incident power and high polarisation purity. An optical chopper was used to modulate the laser signal at a modulation frequency f_1 providing the reference signal for the first lock-in amplifier (SR830 Stanford Research Systems). A 50/50 beam splitter redirects the reflected beam, either from a rotating reference mirror (chopper mirror) or from the sample under test to the photodiode. As the device does not work under normal incidence, a high reflectance mirror was used to redirect the

reflected beam back to the sample and then to the photodiode. At the CGWRR, the probe beam had a diameter of approximately 1.5 mm. The modulation frequency f_2 of the chopper mirror provided the reference signal for the second lock-in amplifier (SR830 Stanford Research Systems).

This differential measurement scheme, which uses a fast modulation between the reference signal reflected from the chopper mirror and the unknown signal reflected by the sample to be measured, reduces the sensitivity to the intensity fluctuations of the laser beam. The detection of the signal was accomplished using a large-area Si-photodiode (Hamamatsu S2386-8K) coupled to an integrating sphere.

3 Results and discussion

In this section, we present our key observations regarding the fabrication and characterisation process of the CGWRR. We will discuss the topographical measurements of the grating structures as well as the reflectivity performance with respect to the design brief.

3.1 Surface topography

In Fig. 6, we present SEM images of a representative structured sapphire sample after ICP etching and SiO$_2$ mask removal. Figure 6a highlights the dimensions achieved during the fabrication process, whilst Fig. 6b shows a lower magnification cross-section image illustrating the quality of the surfaces over a number of ridge features. Due to the difficulty in cleaving sapphire, the end faces of the samples are not ideal; however, this has no impact on the functionality of the CGWRR.

The etching rate of sapphire was 46 nm/min with a selectivity of 1 with respect to the mask material. The sidewall angle is around 73°, a deviation from the 90° design profile, which fortunately according to further simulation studies does not significantly affect the performance of the device.
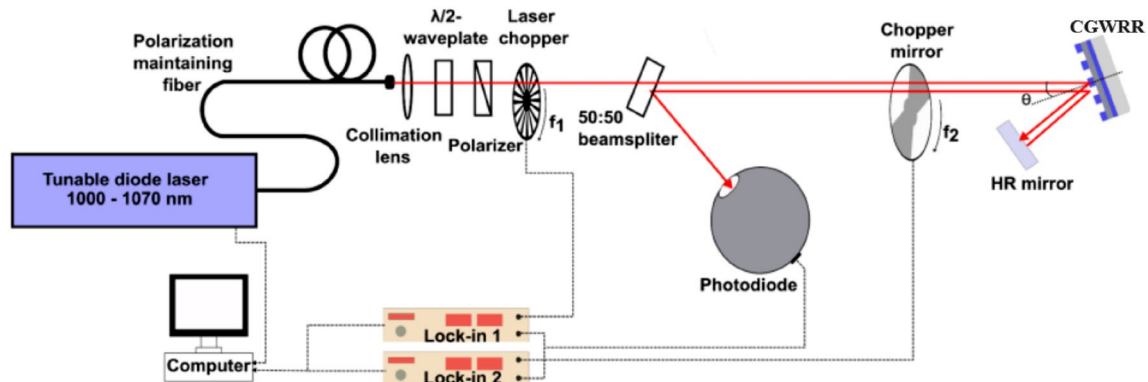

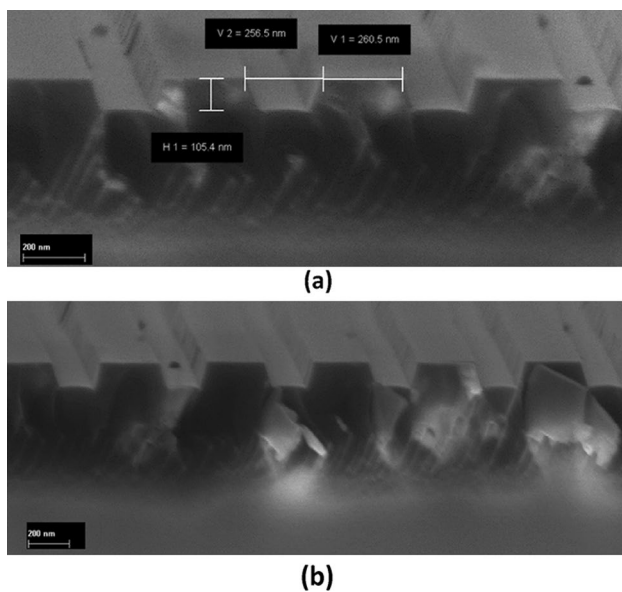**Fig. 5** Reflectivity measurement setup, after [21]

Fig. 6 SEM images in cross-sectional view after ICP etching of sapphire using $SiCl_4/Cl_2/Ar$ chemistry

The cause of the resulting 73° sidewall angle after etching is under investigation and may be related to the crystal-planes' orientation; however, this is an ongoing study, which will be reported in the future work.

AFM measurements were employed to monitor the topography of the grating profile before and after PLD during our process development. A representative example is presented in Fig. 7 where the measured profile of the grating structures before (Fig. 7a) and after PLD (Fig. 7b) confirmed that the deposition is conformal, and the shape of the gratings remains consistent (Fig. 7c).

During the development of the PLD process for the structured sapphire substrates, there were several cases where significant texture in the as-deposited film surfaces was observed, which likely would lead to scattering losses and compromise the performance of these devices [22]. Subsequent tests revealed that it was the laser heating power that was critical for reducing the films' texture. Smoother surfaces were achieved with ~ 22 W of incident CO_2 laser power, leading to significantly improved deposited waveguide film and higher TE and TM resonant reflectance, as will be explained in the next section.

3.2 Reflectivity measurements

Before introducing the CGWRR into a laser cavity, it is necessary to test its reflectance. The spectroscopic setup described in Sect. 2.3 was used to measure the samples' reflectivity as a function of the angle of incidence or wavelength, for the respective polarisation states. Initially, the wavelength of the tuneable diode was set to 1030 nm (i.e.

the central wavelength of the Yb:YAG thin-disc laser) and the CGWRR sample rotated to find the resonance for the TE mode. The resulting resonance angle was found to be 10.5°. Fixing the sample at the optimum angle, the wavelength of the tuneable diode was then scanned to investigate the resonance peak around the wavelength of 1030 nm. The maximum in the TE reflectance was $R_{TE} = 86.9 \pm 0.2\%$ at a wavelength of 1030 nm, whilst the maximum TM reflectance was $R_{TM} = 87.2 \pm 0.2\%$, observed at 1013.5 nm, as shown in Fig. 8a. Also shown in the same figure are the theoretical simulations (using the measured characteristics of the CGWRR-109 nm etching depth, 400 nm Sc_2O_3 thickness, 515 nm period, 50% duty cycle-, and adjusting the AOI to 10.5°) to match the observed performance of the device. Two key characteristics need to be highlighted, the first being that the simulation does not account for reflections from the rear surface of the sapphire substrate, which in practice leads to interference effects on the Fresnel reflection background, and second, the deviation from the ideal reflectance is assumed to be related to imperfect surface quality and differences in the physical dimensions with respect to the specifications. Topographical measurements using AFM showed some texture on the crystalline surface on this grating, which is assumed to be the main cause for the losses (Fig. 8b).

Apart from spectral measurements, where only the wavelength was tuned, we also performed spatial measurements to determine the reflectivity over a 4×4 mm^2 area on the main sample under test. As the sample was mounted on a translation stage, it could be readily moved in the plane of the surface to probe different regions across the grating. For the TE polarisation, we used the resonance wavelength of 1030 nm (Fig. 9a), and for TM polarisation, we used the resonance wavelength of 1013.5 nm (Fig. 9b).

As shown in Fig. 9, instead of obtaining uniform reflectance over the whole area scanned, we observe a peaked distribution for both TE and TM polarisations. The reflectance falls from the maximum values around 87% close to the centre (yellow area) to a base level as defined by the Fresnel surface reflectance. This indicates that the resonance condition is not matched across this whole region of interest, which can be explained by a variation in the thickness of the waveguide layer. A radial variation in the waveguide thickness is inevitable with the PLD setup employed, as the sample and ablation spot positions are static; thus, the deposition profile is defined by the shape of the plasma plume (Fig. 4b).

To confirm that there was a thickness variation across the tested region, we performed spectral measurements away from the centre (e.g. at a position $x = 0$, $y = \sim 1.5$ mm) without changing the AOI of the sample. As shown in Fig. 10, we still observed resonances, however, at down-shifted wavelengths. Moreover, the reflectance was not quite as high as the on-centre measurements, with the off-centre
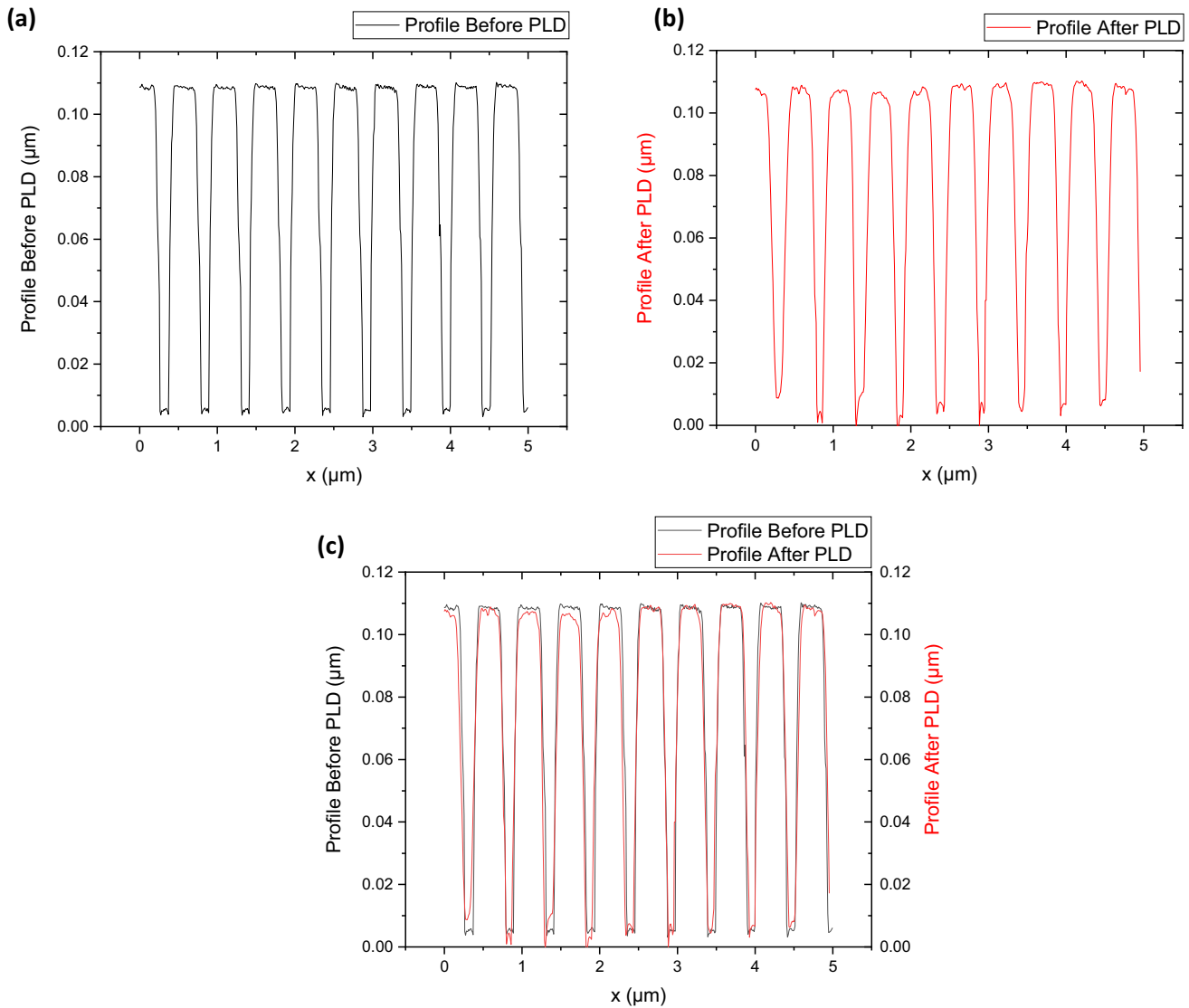
(a)

(b)

(c)

Fig. 7 AFM measurement of grating profile, **a** before PLD, **b** after PLD, and **c** comparable graph of AFM profiles

resonance reflectance being $R_{TE} = 70.1 \pm 0.2\%$ at a wavelength of 1028 nm and $R_{TM} = 73.3 \pm 0.2\%$ at a wavelength of 1013 nm. Based upon simulation results, shown in the same graph, the down-shifted resonance wavelengths can be replicated for a decrease in waveguide thickness by 10 nm, namely Sc$_2$O$_3$ is 390-nm thick in this position, whilst in the centre it is 400-nm thick.

To demonstrate the sensitivity in the resonance wavelength on the film thickness, the results of simulations with 20-nm deviations from the target thickness are presented in Fig. 11.

Apart from the wavelength shift due to thickness variation, we also observed a drop in the reflectivity values between the resonance in the central position ($x = 0$, $y \sim 0$), where reflectivities are $R_{TE} = 86.9 \pm 0.2\%$ and $R_{TM} = 87.2 \pm$ 0.2%, and the resonance at the position ($x = 0$, $y \sim 1.5$ mm), $R_{TE} = 70.1 \pm 0.2\%$ and $R_{TM} = 73.3 \pm 0.2\%$. This can be justified with reference to the graph of the spatial measurements for TE and TM in Fig. 9. Noting that the probe beam diameter is 1.5 mm (1-pixel = $(0.4 \times 0.4$ mm$)^2$) and that only in the central/yellowish area is there reasonable uniformity, we expect to obtain the highest reflectivity under resonance conditions in the centre. Here, the whole beam should essentially interact with the same waveguide thickness. However, moving away from the centre, the beam will sample a graded waveguide thicknesses across its width. Consequently, the result is that the resonance is not perfect across the whole probe beam and an average reflectance is obtained in this area.
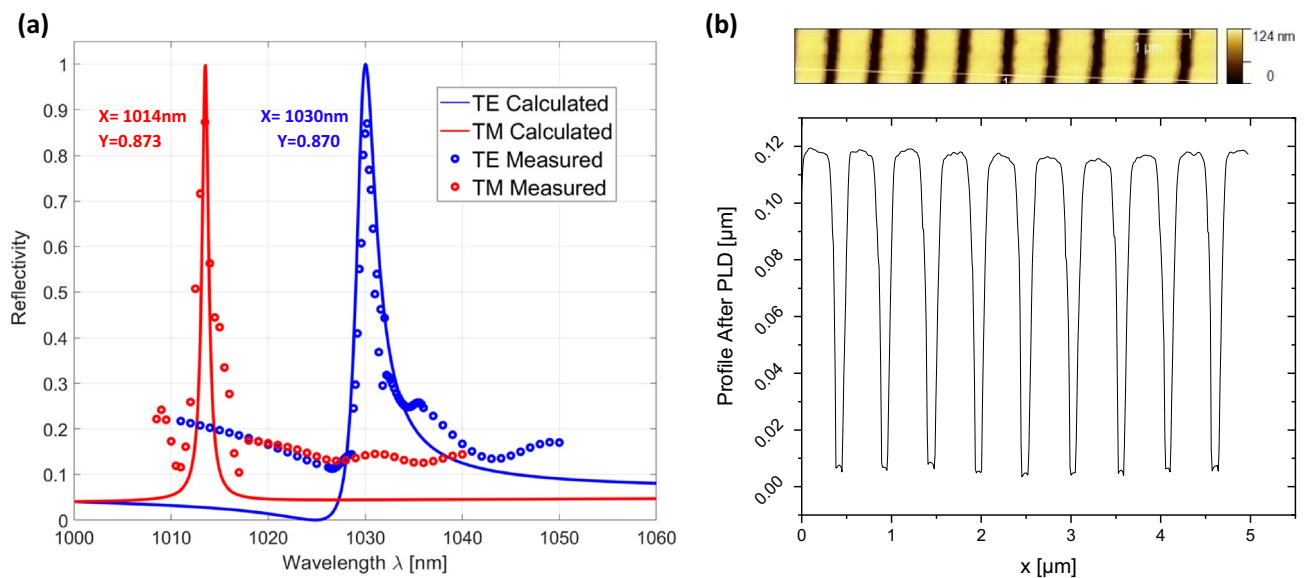
(a)

(b)

Fig. 8 **a** Comparison of calculated and experimental values of spectral reflectivity in TE and TM mode, at a central position on the sample, and **b** AFM measurement of grating profile after PLD
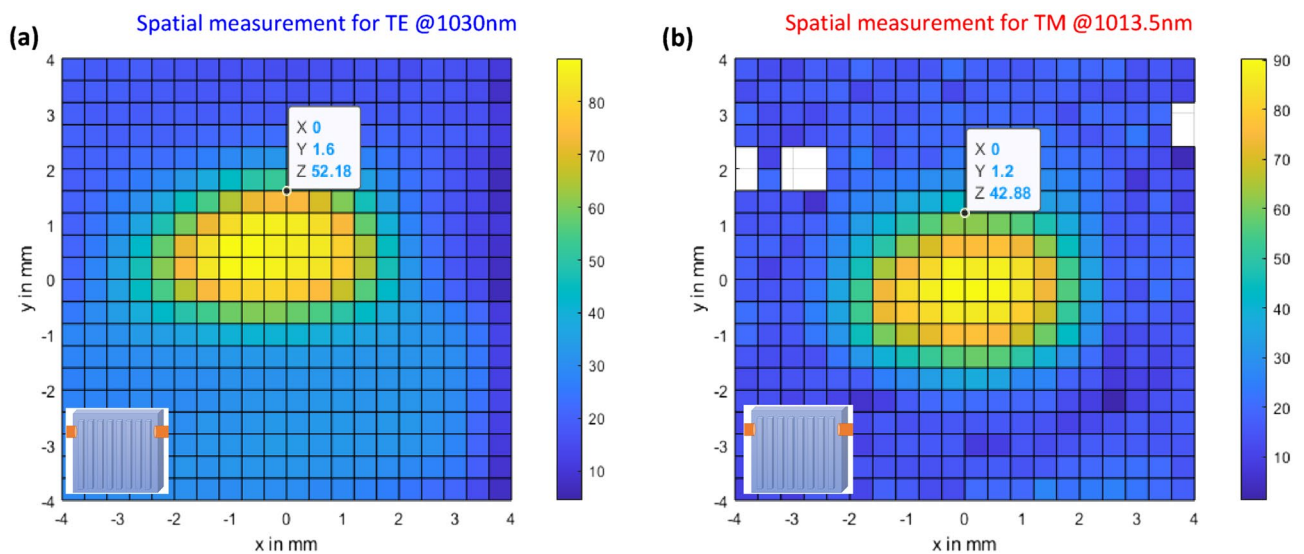
(a)

(b)

Fig. 9 Spatial reflectivity measurements—contour plots at: **a** 1030 nm for TE, and **b** 1013.5 nm for TM

4 Conclusions

In this work, we presented the design, fabrication, and characterisation of the first dielectric crystalline reflectors based on GWS. Rigorous coupled-wave analysis was used to determine the opto-geometrical parameters (i.e. period, etching depth, and film thickness) for operation at 1030 nm. Nanofabrication methods were employed to structure sub-wavelength linear gratings onto sapphire substrates, followed by PLD of a Sc_2O_3 film on top. SEM measurements used to optimise and monitor the etching process verified that an etching rate of 46 nm/min was achieved for the sapphire leading to structures with a 73° sidewall angle. It was confirmed through further simulations that the trapezoidal profile of the sapphire ridges does not affect the performance of the CGWRR. AFM measurements confirmed that conformal growth of Sc_2O_3 was obtained using PLD, realising a consistent grating shape. However, in several cases, during the development process, we observed significant surface texture on the deposited films that led to scattering losses.
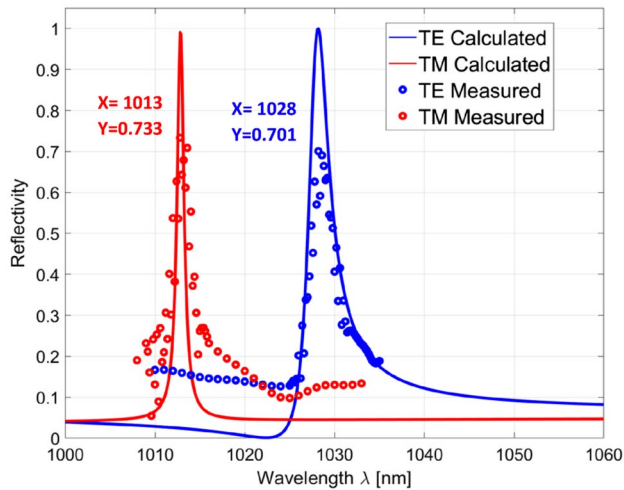
Fig. 10 Comparison of calculated and experimental values of spectral reflectivity in TE and TM mode, at position ($x = 0$, $y = \sim 1.5$ mm)
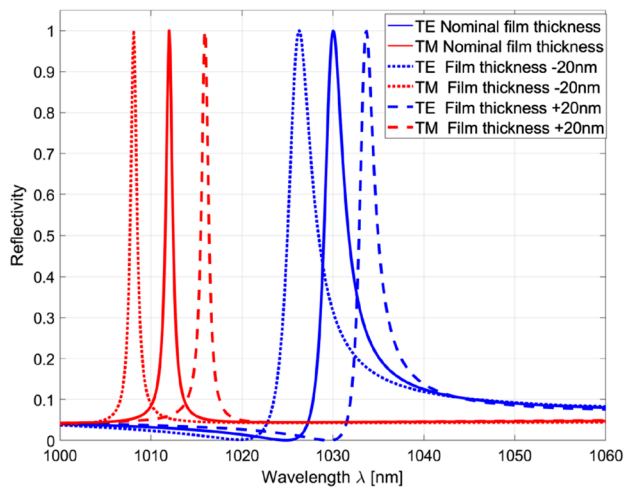

Fig. 11 Simulation of spectral reflectivity dependence on waveguide film thickness

This observation highlighted the need of having excellent control of the fabrication processes, especially that of PLD. With smooth surfaces, the CGWRR performed near to expectations in terms of their TE and TM resonances. Measured TE- and TM-polarisation reflectance demonstrated an achieved resonant reflectivity of ~ 87% ($R_{TE} = 86.9 \pm 0.2\%$ at 1030 nm and $R_{TM} = 87.2 \pm 0.2\%$ at 1013.5 nm) at an angle of incidence of 10.5°. It was discovered that the spatial uniformity of the CGWRR was not ideal, leading to reduced reflectance away from the centre of the samples' surface, which was attributed to thickness variation of the waveguide layer. For future implementations, improved thickness uniformity can be achieved in PLD through scanning of the ablation spot, or the sample, during deposition to average out the shape of

the plasma plume. In conclusion, this study demonstrates the first realisation of an all-dielectric CGWRR. Minor improvements in the fabrication processes and tolerances are required to get closer to the ideal resonance reflection efficiency, as material/scattering losses appear to limit current performance. With refinement of these processes, better device efficiency with substrates that have an order-of-magnitude higher thermal conductivity will be realised, enabling implementation of these narrow-linewidth polarisation-selective reflectors in kW-class lasers.

Author contributions GM and DB contributed equally to writing the manuscript. GM, GG and FL did the fabrication process. GM and DB did the characterization process. DB and MAA did the design. JM, MAA and TG assisted in the preparation of the manuscript. All authors reviewed the manuscript.

Declarations

Competing interests The authors declare no competing interests.

Ethical statement The authors confirm that this material is their own original work, which has not been previously published and is not currently being considered for publication elsewhere. The paper reflects the authors' own research and analysis in a clear and honest manner, without any form of data falsification. The authors properly credited all sources and did not appropriate the work of others.

References

1. D. Rosenblatt, A. Sharon, A.A. Friesem, IEEE J. Quantum Electron. **33**, 2038 (1997)
2. M. Abdou Ahmed, M. Rumpel, A. Voss, T. Graf, Adv. Opt. Technol. **1**, 381 (2012)
3. M. Rumpel, A. Voss, M. Moeller, F. Habel, C. Moormann, M. Schacht, T. Graf, M. Abdou Ahmed, Opt. Lett. **37**, 4188 (2012)

4. M.M. Vogel, M. Rumpel, B. Weichelt, A. Voss, M. Haefner, C. Pruss, W. Osten, M. Abdou Ahmed, T. Graf, Opt. Express **20**, 4024 (2012)

5. M. Rumpel, B. Dannecker, A. Voss, M. Moeller, C. Moormann, T. Graf, M. Abdou Ahmed, Opt. Lett. **38**, 4766 (2013)

6. M. Niraula, R. Magnusson, Opt. Lett. **41**, 2482 (2016)

7. M. Stehlik, G. Govindassamy, J. Zideluns, F. Lemarchand, F. Wagner, J. Lumeau, J. Mackenzie, L. Gallais, Opt. Eng. (2022). https://doi.org/10.1117/1.OE.61.7.070903

8. T.K. Gaylord, M.G. Moharam, Proc. IEEE **73**, 894 (1985)

9. I.C. Botten, M.S. Craig, R.C. McPhedran, J.L. Adams, J.R. Andrewartha, Opt Acta: Int. J. Opt. **28**, 413 (1981)

10. O. Parriaux, V.A. Sychugov, A.V. Tishchenko, Pure Appl. Opt. **5**, 453 (1996)

11. M. Rumpel, M. Abdou Ahmed, A. Voss, T. Graf, Proc. SPIE **8433**, 84331A (2012)

12. G.A. Golubenko, A.S. Svakhin, V.A. Sychugov, A.V. Tishchenko, Sov. J. Quantum Electron. **15**, 886 (1985)

13. S.S. Wang, R. Magnusson, Appl. Opt. **32**, 2606 (1993)

14. S.S. Wang, M.G. Moharam, R. Magnusson, J.S. Bagby, J. Opt. Soc. Am. A **7**, 1470 (1990)

15. A. Sharon, D. Rosenblatt, A.A. Friesem, J. Opt. Soc. Am. A **14**, 2985 (1997)

16. S.S. Wang, R. Magnusson, Opt. Lett. **19**, 919 (1994)

17. I.H. Malitson, F.V. Murphy, W.S. Rodney, J. Opt. Soc. Am. **48**, 72 (1958)

18. O. Medenbach, D. Dettmar, R.D. Shannon, R.X. Fischer, W.M. Yen, J. Opt. A Pure Appl. Opt. **3**, 174 (2001)

19. T.C. May-Smith, A.C. Muir, M.S.B. Darby, R.W. Eason, Appl. Opt. **47**, 1767 (2008)

20. J.J. Prentice, J.A. Grant-Jacob, S.V. Kurilchik, J.I. Mackenzie, R.W. Eason, Appl. Phys. A **125**, 152 (2019)

21. M. Abdou Ahmed, M. Haefner, M. Vogel, C. Pruss, A. Voss, W. Osten, T. Graf, Opt. Express **19**, 5093 (2011)

22. G. Mourkioti, G.A. Govindassamy, F. Li, R.W. Eason, M. Abdou Ahmed, J.I. Mackenzie, EPJ Web Conf. **267**, 02021 (2022)